

Long-range Coulomb interactions and non-hydrodynamic behaviour in thermal quenches in spin ice

Oliver Hart, Marianne Haroche, and Claudio Castelnovo

T.C.M. Group, Cavendish Laboratory, JJ Thomson Avenue, Cambridge CB3 0HE, United Kingdom

(Dated: June 2019)

We study the origin of the plateau in the density of noncontractible pairs of monopoles observed in numerical simulations of thermal quenches in spin ice systems [*Phys. Rev. Lett.* **104**, 107201 (2010)]. We find that the long-range tail of the Coulomb interactions between monopoles plays a central role in the emergence of this metastable state by suppressing the monopole-assisted decay of noncontractible pairs with respect to monopole–antimonopole annihilation. In conjunction with low final quench temperatures, where the system enters a non-hydrodynamic regime in which the monopoles effectively move at terminal velocity in the direction of the local force acting on them, the interactions lead to a metastable plateau that persists in the thermodynamic limit. We demonstrate this using Monte Carlo simulations and mean field population dynamics theory, and we provide an analytical understanding of the underpinning mechanisms at play. When the interactions between monopoles are truncated to finite range, the metastable plateau is still present, but reduces to a finite size effect. We derive the finite size scaling behaviour of the density of noncontractible pairs in the metastable plateau for both short- and long-range interactions, and discuss the implications of our results in experimentally relevant settings.

I. INTRODUCTION

Spin ice materials [1] are a class of three-dimensional frustrated magnets endowed at low temperature with topological properties and an emergent gauge symmetry [2]. Moreover, they harbour collective excitations that take the form of itinerant, point-like defects carrying a net magnetic charge: magnetic monopoles [3]. The nonequilibrium behaviour of these systems is particularly rich and exciting and they can exhibit remarkably long relaxation and response timescales at low temperatures. While a number of attempts have been made to model and understand the origin of the dynamical behaviour in spin ice materials, the complete picture arguably remains beyond our grasp.

In this paper, we make progress by investigating the specific setting of thermal quenches in classical spin ice [4], and we uncover the mechanisms that underpin the formation of the observed metastable plateau in which monopoles form noncontractible pairs. We find that the phenomenon is rooted in two key ingredients: (i) the long-range nature of the Coulomb interaction between the monopoles; and (ii) the fact that low temperature thermal quenches in spin ice are able to access a non-hydrodynamic regime that increases the decay rate of the free monopole density in the system.

In providing a complete understanding of thermal quenches, our results demonstrate that the plateau reduces to a finite size effect in the presence of interactions of finite range. Hence, the experimental observation of a metastable plateau corresponding to a finite density of noncontractible pairs in spin ice is direct evidence of the long-range nature of the interactions between the monopoles. This adds one important experimental avenue to study these interactions, whose range has thus far been probed only via the field-dependence of unbinding of monopole pairs [5], and indirectly via the appearance of a liquid-gas phase diagram [3].

Our findings are particularly timely thanks to the recent experimental claim that a state rich in noncontractible pairs can be generated in classical spin ice materials $\text{Dy}_2\text{Ti}_2\text{O}_7$ and $\text{Ho}_2\text{Ti}_2\text{O}_7$ [5] using a so-called avalanche quench protocol [6].

The paper is structured as follows. We start by reviewing

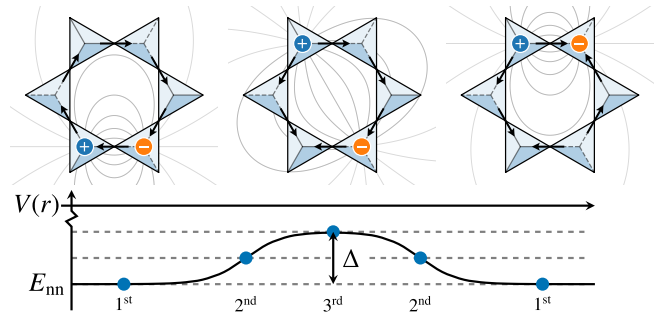


FIG. 1. Schematic depiction of a noncontractible monopole–antimonopole pair, responsible for the metastable plateau in monopole density, observed following a thermal quench to low temperatures in classical spin ice. The activated decay of the pair requires separating its members up to third-neighbour distance, as shown in the central figure, costing an energy Δ (in isolation) due to their mutual Coulombic attraction. The pair is then free to annihilate, as shown for example in the rightmost figure.

the background on thermal quenches in classical spin ice and by summarising the main results obtained in this work in Sec. II. We then provide an overview of the models we consider in Sec. III, and we present our Monte Carlo results in Sec. IV, including a finite size scaling analysis of the density of noncontractible pairs in the metastable plateau. Sec. V is devoted to the use of mean field population dynamics to understand the differences in behaviour between the different models and types of interaction. We draw our conclusions and highlight the relevance of our results to recent experiments in Sec. VI.

II. BACKGROUND AND SUMMARY OF RESULTS

Dipolar spin ice systems have been predicted to exhibit dynamically-arrested, monopole-rich, metastable states following appropriate thermal and field quenches [4, 7]. Ref. 4 recognised that at the heart of the dynamical arrest lies the formation of so-called noncontractible pairs: a monopole and

an antimonopole sitting next to one another, separated by a spin whose reversal does not lead to their annihilation. As a result, the two defects become bound to one another and are unable to move throughout the lattice without separating—a process that costs Coulomb energy due to the mutual attraction between the two opposite charges. This activation energy barrier explains why a noncontractible pair per se is metastable.

In general, two decay channels are available to noncontractible pairs. Firstly, they can separate and annihilate somewhere else on the lattice at the cost of paying an activation energy barrier; the smallest barrier to such activated decay processes requires separating the pair up to third-neighbour distance, as shown in Fig. 1. Alternatively, pairs can undergo monopole-assisted (radioactive) decay: when the pair is hit by a stray (free) monopole, this causes the annihilation of the oppositely charged member of the pair, thus freeing up its partner [4], as in Fig. 2. The latter process does not incur an energy barrier and does not change the density of free monopoles.

The mere existence of noncontractible pairs in the system does not warrant the appearance of a macroscopic metastable state. Indeed, when free monopoles are abundant, non-activated (fast) radioactive decay is the leading relaxation channel. It is only when the system undergoes a “population inversion” (with respect to, say, random/high-temperature initial conditions), where noncontractible pairs become the dominant species in the overall monopole density, that the activation energy barrier for decay can induce a long-lived metastable plateau at low temperatures. This is indeed what one observes in numerical simulations of dipolar spin ice, following appropriate thermal quenches [4].

The aforementioned population inversion is key to the metastable plateau. Its origin was however not investigated in Ref. 4 and is the subject of the present work. We find that it ultimately rests on the long-range tail of the Coulomb interaction between monopoles. This can be qualitatively understood as being due to the energetic bias in the motion of monopoles in the far field. Monopole–antimonopole collision events are subject to a Coulombic charge–charge attraction ($\propto r^{-2}$), whereas collisions between a free monopole and a noncontractible pair are subject to weaker charge–dipole interactions ($\propto r^{-3}$). This leads to a bias that increases the likelihood of free monopoles annihilating (or forming new noncontractible pairs) over their chance of annihilating existing noncontractible pairs via radioactive decay. Further, since the final temperature in the thermal quenches is much less than all other energy scales in the problem, the system enters a non-hydrodynamic regime where the monopoles move at terminal velocity in the direction of the local force acting on them. This allows the system to violate the law of formal kinetics [8] and exhibit a decay of monopole density parametrically faster than inverse time. The combination of the long-range bias and ‘terminal velocity’ motion of free charges leads to a rapid decay of the free monopole density in the system which ultimately causes the population inversion at the root of the finite-density metastable plateau observed in numerical simulations.

This behaviour is most remarkable. By altering the dynamics of what is ultimately a transient regime, spin ice is able to enter a metastable state whose lifetime for experimentally relevant

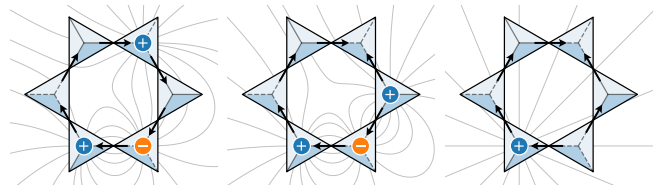


FIG. 2. Schematic depiction of monopole-assisted (radioactive) decay of a noncontractible pair. A free monopole annihilates with the oppositely charged member of the stationary noncontractible pair, thereby freeing up its partner. All moves shown lower the energy of the system and so radioactive decay is the dominant decay avenue for noncontractible pairs when free monopoles are abundant in the system.

temperatures and system sizes may well exceed any realistically accessible timescales.

We verify this scenario through extensive numerical Monte Carlo simulations of thermal quenches in spin ice with nearest-neighbour spin–spin interactions and long-range Ewald-summed magnetic Coulomb interactions between defective tetrahedra [9]. Upon truncating the Coulomb interactions to finite range, the long-range bias is removed. We find that the finite-density metastable plateau correspondingly disappears in the thermodynamic limit. These findings are corroborated by directly simulating mutually interacting magnetic charges hopping on a diamond lattice, for which qualitatively similar behaviour is observed.

To supplement the numerics, we provide an analytical understanding of both the value of the plateau in the thermodynamic limit and its finite size scaling using mean field population dynamics, treating the system as Coulomb liquid of magnetic charges. We show how the ratio of the rate of radioactive decay to the rate of charge–charge annihilation underpins both the finite size scaling exponent in the case of truncated interactions, and the density at which the plateau occurs in the long-range case.

III. MODELS

In this work, we contrast the effect of truncating the Coulomb interactions between monopoles in spin ice with the same truncation in a model of magnetic charges hopping on a diamond lattice. This allows us further clarity in ascertaining the role of the spin configuration underlying each configuration of monopoles. Therefore, we introduce the following two systems.

A. Classical spin ice

The canonical model of classical spin ice (CSI) consists of exchange (J) and dipolar (D) interactions between classical Ising spins $S_i \in \{-1, +1\}$ living on the sites of a pyrochlore

lattice [10, 11]

$$H_d(\{S_i\}) = \frac{J}{3} \sum_{\langle ij \rangle} S_i S_j + D \sum_{\langle ij \rangle} \left[\frac{\mathbf{e}_i \cdot \mathbf{e}_j}{|\mathbf{r}_{ij}|^3} - \frac{3(\mathbf{e}_i \cdot \mathbf{r}_{ij})(\mathbf{e}_j \cdot \mathbf{r}_{ij})}{|\mathbf{r}_{ij}|^5} \right] S_i S_j, \quad (1)$$

where \mathbf{e}_i are the local easy axes of the spins. For the majority of this work, we use an effective Hamiltonian in which the exchange and dipolar interactions between the spins are retained only at nearest-neighbour level, and farther range couplings are accounted for effectively in the form of a pairwise interaction $V(\{Q_a\})$ between tetrahedral charges Q_a (defined below). First, we consider the case where V assumes the form of an Ewald-summed, long-range Coulomb coupling between defective tetrahedra (i.e., monopoles, as well as all-in, all-out tetrahedra) [3]. The resulting spin Hamiltonian takes the form

$$H_c(\{S_i\}) = J_{\text{eff}} \sum_{\langle ij \rangle} S_i S_j + E_{\text{nn}} \sum_{a \neq b} \frac{Q_a Q_b}{r_{ab}}, \quad (2)$$

where i, j index the sites of the pyrochlore lattice, a, b index the tetrahedra and $r_{ab} = |\mathbf{r}_a - \mathbf{r}_b|/r_{\text{nn}}$ is the distance between the centres of tetrahedra a and b in units of the distance between neighbouring tetrahedra. The charge on tetrahedron a is $Q_a = \pm \sum_{i \in a} S_i/2$, where the sign depends on the sublattice that a belongs to. The charge Q_a therefore assumes the values $Q_a \in \{0, \pm 1, \pm 2\}$. We use the convention that a positive charge corresponds to a majority of spins pointing out of a given tetrahedron. Two oppositely-charged monopoles on neighbouring sites have a Coulomb energy E_{nn} (in an infinite system). Throughout the manuscript we use an effective exchange coupling $J_{\text{eff}} = 1.463$ K [12] and nearest-neighbour Coulomb energy $E_{\text{nn}} = 3.06$ K, appropriate for the classical spin ice compound $\text{Dy}_2\text{Ti}_2\text{O}_7$. Such an effective description (2) neglects quadrupolar corrections to the interactions between monopoles $V(\{Q_a\})$ [13]. With these parameters, the macroscopically degenerate ground state manifold corresponds to the charge vacuum, $Q_a = 0, \forall a$, i.e., a 2 in-2 out configuration of spins on each tetrahedron.

The nearest-neighbour exchange interaction between spins may alternatively be viewed as a chemical potential of size $2J_{\text{eff}}$ for the monopoles (namely, charges $Q_a = \pm 1$):

$$J_{\text{eff}} \sum_{\langle ij \rangle} S_i S_j = 2J_{\text{eff}} \sum_a Q_a^2 - N_s J_{\text{eff}}. \quad (3)$$

In a finite system containing L^3 cubic unit cells, the total number of spins is $N_s = 16L^3$, and the number of tetrahedra is $N_t = 8L^3$. We note that there also exists a long-range Coulomb interaction between monopoles of entropic origin [14].

To test the role of the long-range tail of the Coulomb interaction in establishing the population inversion, we also consider a similar model where the interactions $V(\{Q_a\})$ between monopoles are truncated at nearest-neighbour distance:

$$H_t(\{S_i\}) = J_{\text{eff}} \sum_{\langle ij \rangle} S_i S_j + \Delta \sum_{\langle ab \rangle} Q_a Q_b. \quad (4)$$

Such a nearest-neighbour interaction between monopoles allows for the formation of noncontractible pairs without inducing any long-range energetic bias in the motion of the monopoles [15].

Separating an isolated pair of nearest-neighbour monopoles with charge $Q = \pm 1$ in this model costs an energy Δ . To preserve the behaviour of the system (primarily its ground state), the truncation of the interactions must be done with care. We choose the value of Δ such that the energy barrier to separating a noncontractible pair around a hexagonal plaquette (as depicted in Fig. 1) is equal in the truncated and long-ranged cases:

$$\Delta = E_{\text{nn}} \left(1 - \sqrt{\frac{3}{11}} \right) \approx 1.46 \text{ K}. \quad (5)$$

Such a choice preserves the charge vacuum ground state, and since the energy barrier for the activated decay of noncontractible pairs is equal for both types of interaction, the demise of a possible metastable plateau will occur at similar times in the two cases. The difference between the single spin flip dynamics of the two Hamiltonians, H_c and H_t , therefore rests solely in the long-range energetic bias in the motion of monopoles across the system.

B. Charges on diamond lattice

To identify the role of the spin configuration underlying each monopole configuration, we also consider two further effective models of charges Q_a hopping on a diamond lattice, thereby removing any entropic effects and blocked directions associated with the spins. We restrict our simulations to the relevant charge values $Q_a \in \{0, \pm 1, \pm 2\}$ only. These charge models (CM) also allow for a more direct comparison with our analytical mean field modelling (see Sec. V), which largely neglects the aforementioned complications associated with the spinful description of the system dynamics.

In the case of long-range interactions between the charges, we use the Hamiltonian

$$H_c^{\text{CM}}(\{Q_a\}) = 2J_{\text{eff}} \sum_a Q_a^2 + E_{\text{nn}} \sum_{a \neq b} \frac{Q_a Q_b}{r_{ab}}, \quad (6)$$

subject to the constraint that each site may not be occupied by more than two charges.

The Hamiltonian (6) must be further supplemented by rules which govern the dynamics of the charges, in order to take into account the effect of noncontractible pairs. Namely, when two opposite (single) charges come into nearest-neighbour contact, there exists some finite probability, p_{nc} , of forming a noncontractible pair. If a noncontractible pair is formed, it is then not possible for the charges to annihilate along their common bond. At finite temperature, their activated decay can be accounted for by associating an energy barrier Δ with such a decay.

The probability p_{nc} can be estimated by counting the number of spin configurations compatible with two oppositely charged monopoles on adjacent tetrahedra, and taking the fraction thereof that correspond to a noncontractible pair. If we consider

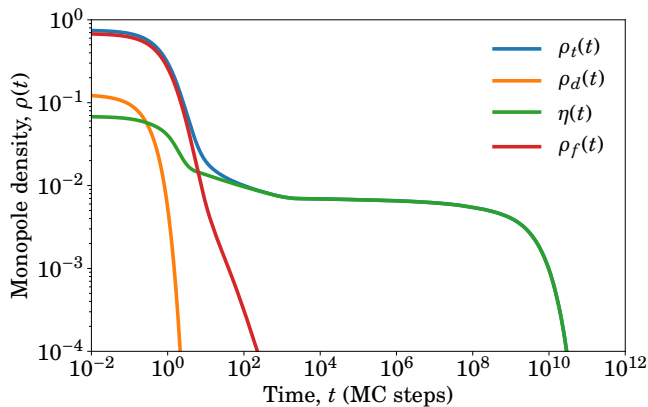


FIG. 3. Monte Carlo simulations of a thermal quench in spin ice subject to Ewald-summed Coulomb interactions between monopoles (Hamiltonian (2), system size $L = 22$, i.e., 170 368 spins) from infinite temperature down to $T = 0.06$ K. The curves show the evolution of the averaged total density of monopoles per tetrahedron ρ_t (blue), the free monopole density ρ_f (red), the density of monopoles forming noncontractible pairs η (green) and the double charge density ρ_d (orange). Time is expressed in units of Monte Carlo steps per site, and the densities are averaged over 4096 histories.

the minimal cluster of two tetrahedra only (7 spins in total), one finds that the relevant fraction is $p_{nc} = 1/10$ [4]. Extending the calculation to larger cluster does not lead to significant variation in this value; for example, considering a full hexagon of tetrahedra involving the two monopoles gives $p_{nc} = 41/406$. Further, small perturbations in p_{nc} do not appreciably modify the system dynamics.

For the case of truncated interactions between the tetrahedral charges, the Hamiltonian becomes

$$H_t^{\text{CM}}(\{Q_a\}) = 2J_{\text{eff}} \sum_a Q_a^2 + \Delta \sum_{\langle ab \rangle} Q_a Q_b, \quad (7)$$

where again we enforce that $|Q_a| \leq 2$ for all sites a . The rules governing the dynamics of the two charge models, H_c^{CM} and H_t^{CM} , are identical. Again, the difference between the two charge models lies in the long-range energetic bias associated with the Coulomb interaction.

IV. MONTE CARLO SIMULATIONS

A. Classical spin ice

1. Long-range Coulomb interactions

In Fig. 3 we show the monopole density evolution following a thermal quench, as in Ref. 4, simulated using the modified Monte Carlo code instead of the conventional dipolar Monte Carlo. We use single spin flip dynamics and the Waiting Time Method [16, 17] to access long simulation times at low temperatures (see App. A for some details specific to our simulations). The system is initially prepared in a paramagnetic phase at infinite temperature; then at $t = 0$ the temperature is

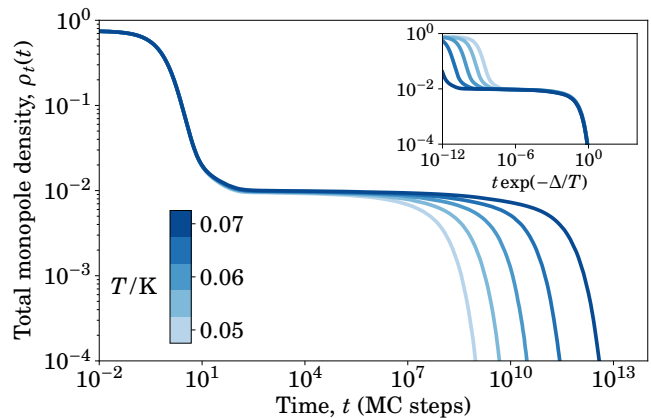


FIG. 4. Monte Carlo simulations of the total density of monopoles ρ_t in the case of long-range Coulomb interactions between monopoles, after a thermal quench from infinite temperature down to final temperatures $T = 0.05$ – 0.07 K (in equidistant steps) for a system of size $L = 8$, i.e., 8192 spins. The densities are averaged over 4096 runs. Inset: the same curves plotted after rescaling the time axis by a factor $\exp(\Delta/T)$, where $\Delta \approx 1.46$ K is the Coulomb energy barrier incurred by separating two monopoles around a hexagonal plaquette, showing an excellent collapse of the long-time decay of the monopole density.

set to its target value, $T \ll J_{\text{eff}}$, and we start measuring various monopole densities as a function of time. These densities are then averaged over many histories with different random initial conditions sampled from the infinite temperature ensemble. We find good agreement with the dynamical arrest observed in Ref. 4: rather than rapidly equilibrating to a monopole-sparse state, we observe the emergence of a metastable plateau in the monopole density due to noncontractible monopole–antimonopole pairs.

Specifically, we measure the total monopole density (monopoles per tetrahedron) in the system, ρ_t , counting all-in and all-out tetrahedra as doubly occupied sites; the fraction of such doubly occupied sites, ρ_d ; the density of monopoles forming noncontractible pairs, η ; and the ‘free’ monopole density [18] $\rho_f \equiv \rho_t - \eta$, i.e., the density of monopoles that do not form noncontractible pairs. A noncontractible pair is *defined* as a pair of adjacent, oppositely-charged monopoles for which the reversal of the intervening spin shared by the two tetrahedra does not lead to annihilation of the pair.

In isolation, the barrier to activated decay of a noncontractible pair is $\Delta \approx 1.46$ K. In the presence of a finite density η of other noncontractible pairs, the distribution of energy barriers is broadened around a mean value of Δ due to dipole–dipole interactions between the pairs. Given that the Coulombic approximation to the monopole–monopole interaction neglects quadrupolar corrections, we expect the distribution of such energy barriers to be more sharply peaked than in the dipolar case. This is indeed confirmed by the excellent collapse of the long-time monopole density decay for various temperatures upon rescaling the time axis by a factor $\exp(\Delta/T)$, as illustrated in Fig. 4.

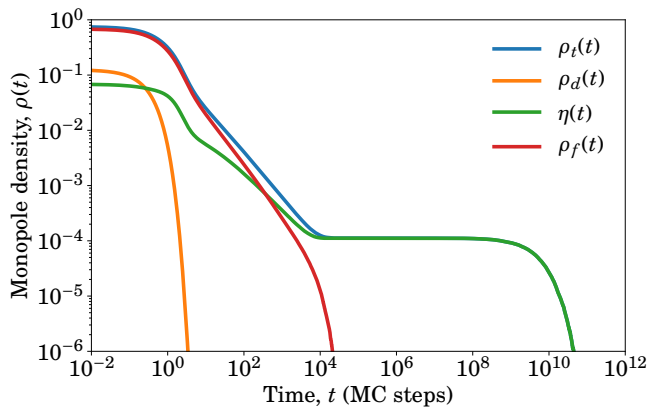


FIG. 5. Monte Carlo simulations of a thermal quench in spin ice where the interactions between monopoles are truncated to nearest-neighbour distance (Hamiltonian (4), system size $L = 16$, i.e., 65 536 spins) from infinite temperature down to $T = 0.06$ K. Time is expressed in units of Monte Carlo steps per site, and the densities are averaged over 4096 histories. The metastable plateau due to noncontractible pairs of monopoles remains present, but occurs at lower densities and at later times than in the case of long-range interactions (cf. Fig. 3).

2. Truncated interactions

In Fig. 5 we plot the various monopole densities for an identical thermal quench for the case of truncated interactions between monopoles. A metastable plateau remains present in the dynamics of the system, and once again the behaviour of the monopole densities tells us that it is clearly due to noncontractible pairs. The plateau however occurs at substantially lower densities and the onset occurs at later times when compared with the long-range interacting system.

The decay of the monopole density at long times collapses for a range of temperatures upon rescaling the time axis by a Boltzmann factor $\exp(\Delta/T)$, as illustrated in the inset of Fig. 6, confirming that the thermally activated decay of noncontractible pairs is again responsible for the eventual demise of the plateau at a time $\tau_{nc} \sim \exp(\Delta/T)$. Once a given pair has separated, the two constituent monopoles may find each other and annihilate by performing a random walk, the shortest of which is around a single hexagonal plaquette. Since the noncontractible pairs do not interact beyond a fixed, finite separation, the energy barriers are δ -distributed about Δ and the decay of the plateau is a perfect exponential.

3. Comparison and finite size scaling

In Fig. 7 we plot the noncontractible pair density as a function of time, $\eta(t)$, for all three types of interaction introduced in Sec. III A: Ewald-summed dipolar interactions between spins, Ewald-summed Coulomb interactions between monopoles, and truncated (nearest-neighbour) interactions between monopoles.

In each of the three cases, the time evolution of $\eta(t)$ can be decomposed into four dynamical regimes. The first occurs over timescales $t \lesssim 10$ (time being measured in Monte Carlo steps

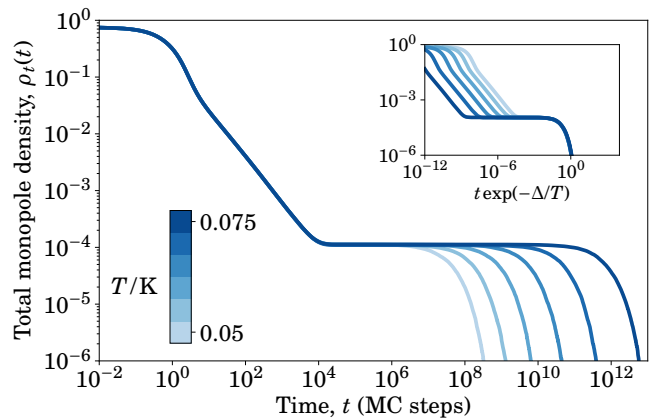


FIG. 6. Monte Carlo simulations of the total density of monopoles ρ_t in the case of truncated interactions between monopoles, after a thermal quench from infinite temperature down to various temperatures $T = 0.05$ – 0.075 K (in equidistant steps) for a system of size $L = 16$, i.e., 65 536 spins. The densities are averaged over 4096 runs. Inset: the same curves plotted after rescaling the time axis by a factor $\exp(\Delta/T)$, showing an excellent collapse of the long-time decay.

per site) and corresponds to the rapid decay of doubly occupied sites—the large exchange energy cost associated with double occupancy ($2J_{\text{eff}}$) and their ability to decay spontaneously ensures that such configurations decay rapidly (exponentially fast in time, see App. C for details). The second regime is where the differences between the three interaction types become manifest. In all cases we observe a much slower decay of the noncontractible pair density once the double monopoles have been removed from the system. However, the rate of decay and the timescales over which this decay occurs are vastly different for the truncated versus long-range interacting models. In the Coulomb and dipolar cases, the long-range nature of the interactions leads to an energetic bias which favours monopole–antimonopole (charge–charge) annihilation over radioactive decay of noncontractible pairs (charge–dipole). This means that (i) the free monopoles in the system vanish more quickly, and, correspondingly, (ii) noncontractible pairs are removed more slowly than in the case of truncated interactions. Since the plateau forms when there are no free monopoles left in the system, point (i) gives rise to the earlier onset of the plateau, while point (ii) implies that the plateau forms at a higher density. The third regime is the metastable plateau, where the system contains essentially only noncontractible pairs. The final regime corresponds to the activated decay of noncontractible pairs at a time $\tau_{nc} \sim \exp(\Delta/T)$. By construction, the decay occurs at similar times for the systems with truncated and long-range Coulomb interactions. The difference in the decay times between the Coulomb and dipolar cases is due to the larger variance in energy barriers for activated decay of the pairs in the latter case. Indeed, one may model the decay of the plateau by assuming a Gaussian distribution of energy barriers, $P(\epsilon)$, with mean Δ and width σ . The activated decay of the noncontractible pair density $\eta(t)$ is then approximated as $\eta(t) = \int d\epsilon P(\epsilon) e^{-t/\tau(\epsilon)}$, where the decay time $\tau(\epsilon) \propto e^{\epsilon/T}$. The values $\sigma_d \approx 0.1$ K [4], $\sigma_c \approx 0.03$ K and $\sigma_t \approx 0$, lead to

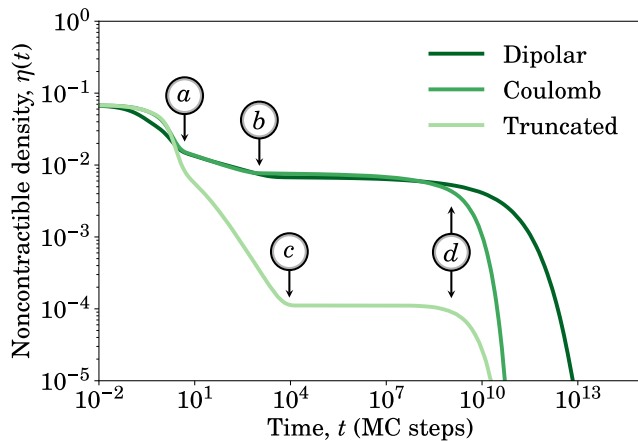


FIG. 7. Comparison of noncontractible pair densities $\eta(t)$ for the three types of interaction for a thermal quench from infinite temperature down to $T = 0.06$ K (system size $L = 16$, i.e., 65 536 spins). Time is expressed in units of Monte Carlo steps per site, and the densities are averaged over 4096 runs. The markers labelled *a*, *b*, *c*, and *d* identify the boundaries between the four dynamical regimes discussed in the main text. At (*a*), nearly all doubly occupied sites have been removed from the system. Points (*b*) and (*c*) mark the onset of the metastable plateau for the cases of long-range and truncated interactions, respectively. At (*d*), the noncontractible pairs decay via thermal activation.

the best fit of the Monte Carlo data (not shown).

Notice that, in systems of finite size, the appearance of a noncontractible plateau in the averaged monopole density is, in fact, unavoidable. On the one hand, the probability that all free monopoles annihilate before all noncontractible pairs have decayed is finite; and, if this happens, the only decay process left for the noncontractible pairs is activated decay. On the other hand, even when the last two monopoles in the system are free, there exists a finite probability of forming a new noncontractible pair, rather than annihilation, when the two monopoles come into nearest-neighbour contact. The latter process places a hard nonzero lower bound on the density of the noncontractible plateau of $O(1/L^3)$, which is purely a finite size effect.

In order to understand the origin of the plateau and the difference between the truncated and long-range cases, we ought therefore to look at the finite size scaling behaviour of the plateau density. Figure 8 shows the noncontractible monopole density in the plateau, $\eta_p(L)$, for systems of different sizes (parameterised by the linear system size L) and the same final quench temperature $T = 0.06$ K. We perform a fit to the scaling ansatz $\eta_p(L) - \eta_p(\infty) \sim L^{-\nu}$, to extract the exponent ν , the value of the plateau in the thermodynamic limit, $\eta_p(\infty)$, and the constant of proportionality. The form of this scaling ansatz is justified later in Sec. V, where we show that a power law decay of the free monopole density with time implies power law scaling of the metastable plateau density with system size. Hence, the scaling ansatz only applies once any transient (non-power law) behaviour of $\rho_f(t)$ at short times has subsided. For dipolar interactions between spins, it is not numerically feasible to access system sizes sufficiently large to observe

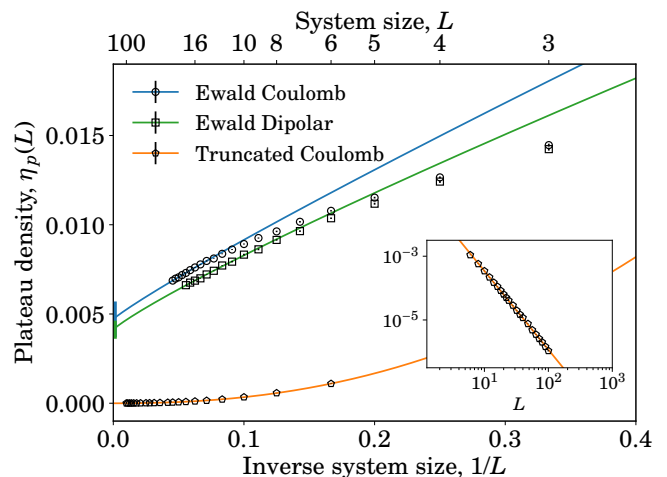


FIG. 8. Finite size scaling of the plateau in noncontractible monopole density $\eta_p(L)$ for long-range Coulomb and truncated (nearest-neighbour) interactions between monopoles, and long-range dipolar interactions between spins. The data are averaged over at least 4096 histories. The lines are fits to the scaling ansatz $\eta_p(L) - \eta_p(\infty) \sim L^{-\nu}$, while the symbols represent the Monte Carlo data. The corresponding error bars are smaller than the width of the fit lines. In the truncated case (system sizes $L = 6$ –100 inclusive), the data are consistent with a plateau that vanishes in the thermodynamic limit. This is verified using a log-log plot of the plateau density against system size L in the inset. Conversely, the long-range Coulomb ($L = 3$ –22 inclusive) and dipolar ($L = 3$ –18 inclusive) cases appear to exhibit a nonvanishing noncontractible pair density in the metastable plateau in the thermodynamic limit: $\eta_p(\infty) = 4.7(9) \times 10^{-3}$ and $\eta_p(\infty) = 4.1(5) \times 10^{-3}$, respectively.

an asymptotic power law decay regime of the free monopole density. We nevertheless provide a fit to the data in this case, but it should be noted that the resulting parameters are subject to some degree of systematic error. In the case of Coulomb interactions between the monopoles, such asymptotic power law decay of $\rho_f(t)$ is observed in systems of size $L \geq 14$ (i.e., 43 904 spins), and correspondingly only these data are included in the scaling analysis.

The inset of Fig. 8 demonstrates that the metastable plateau in the truncated case is indeed a finite size effect: the number of noncontractible pairs in the plateau increases subextensively with the size of the system, $\nu \simeq 2.46$, and the density $\eta_p(\infty)$ is consistent with a vanishing value in the thermodynamic limit. By contrast, in the case of long-range interactions, the number of noncontractible pairs in the plateau scales *extensively* with system size, with subleading, subextensive contributions. Hence, the density of the plateau in the long-range case tends asymptotically towards a finite value, also shown in Fig. 8. The subextensive corrections give rise to the L -dependence of the plateau density. The finite size scaling exponent in this case is $\nu = 0.9(3)$.

We shall attempt to understand the origin of the different behaviours and exponents by modelling the time evolution of the system using mean field population dynamics in Sec. V.

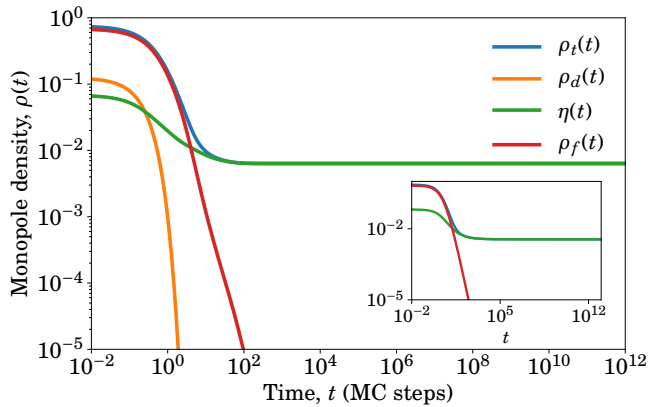


FIG. 9. Monte Carlo simulations of charges hopping on the diamond lattice subject to long-range Coulomb interactions (Hamiltonian (6), system size $L = 22$, i.e., 170 368 spins) from infinite temperature down to zero temperature. Time is expressed in units of Monte Carlo steps per site, and the data are averaged over 4096 histories. The analytic solution, (B2), to the mean field equations for the charge densities is shown in the inset for comparison.

B. Charges on diamond lattice

1. Long-range Coulomb interactions

Moving to the charge description, characterised by the CM Hamiltonian (6), $H_c^{\text{CM}}(\{Q_a\})$, we obtain the results shown in Fig. 9 for a thermal quench down to zero temperature, $T = 0$ [19]. The initial distribution of the charges is set using an infinite temperature distribution of spins on the bonds of the diamond lattice, i.e., using the same initial conditions as in Sec. IV A. After initialisation of the system, all reference to an underlying spin configuration is removed, and the time evolution is determined by the dynamical rules laid out in Sec. III B. The only difference therefore between the charge model and spin ice is the dynamical constraints imposed by the spins in the latter. As in the case of the spinful simulations, we measure the various monopole densities as functions of time after the thermal quench and average over histories.

In this case, we observe a plateau at finite density which persists indefinitely since the noncontractible pairs cannot undergo activated decay at zero temperature. However, contrasting Figs. 3 and 9, there are some quantitative differences between the dynamics of the charge and the spin models. In particular, the decay of free monopoles occurs much more quickly in the charge model. This implies that the onset of the plateau occurs significantly earlier in time than in CSI.

2. Truncated interactions

As shown in Fig. 10, in the case of truncated interactions between charges we again observe a plateau that occurs at later times and at lower densities than in the long-range interacting case (Fig. 9). The free monopole density decays approximately as $1/t$ in the long-time limit, i.e., after the double monopoles

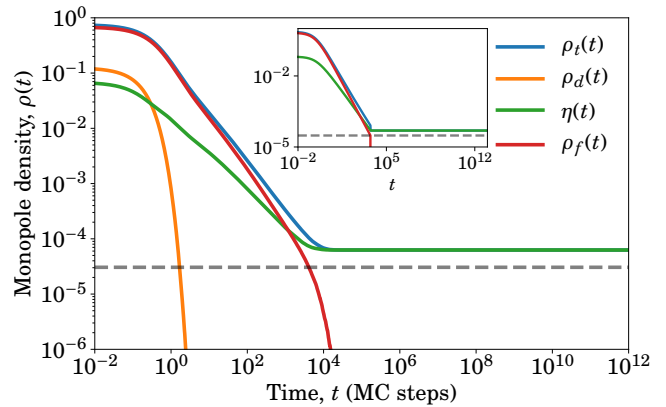


FIG. 10. Monte Carlo simulations of charges hopping on the diamond lattice subject to truncated (nearest-neighbour) interactions (Hamiltonian (7), system size $L = 16$, i.e., 65 536 spins) from infinite temperature down to zero temperature. Time is expressed in units of Monte Carlo steps per site, and the data are averaged over 4096 histories. The analytic solution, (13), to the mean field equations for the charge densities is shown in the inset for comparison. The dashed lines indicate the threshold density corresponding to the removal of free charges in a system of finite size, $\rho_* = 1/N_t$.

have been removed from the system, while the noncontractible pair density decays also as a power law in time, but with a smaller exponent. The power law decay of these quantities is cut off when the free monopoles drop below $O(1/L^3)$ density, shown by the dashed line in Fig. 10. The remaining noncontractible pairs in the system can only further decay by thermal activation and the noncontractible plateau is thus established at this time.

3. Comparison and finite size scaling

The finite size scaling of the plateau in the case of charges hopping on the diamond lattice is presented in Fig. 11. We observe that, as in the case of the spins, the long-range interacting case tends towards a finite plateau density in the thermodynamic limit, while the plateau is merely a finite size effect in the case of truncated interactions between the charges, i.e., $\lim_{L \rightarrow \infty} \eta_p(L) = 0$ with $\nu \approx 2.28$.

These findings corroborate the conclusions of Sec. IV A 3 pertaining to classical spin ice. In particular, that the plateau is not a finite size effect in the case of long-range Coulomb interactions between charges. Since the subleading corrections decay more quickly in the charge description, $\nu = 1.8(4)$, we are able to make this claim on even stronger terms.

The fact that the finite size scaling of the plateau, i.e., the exponent ν , differs significantly between the spinful and charge descriptions for the long-range case, while it is very similar for the spinful and charge descriptions for truncated interactions, is a puzzle that we shall attempt to understand in the following Section. Indeed, we will see that one can achieve a great deal of analytical insight into the observed behaviour by means of appropriate mean field modelling.

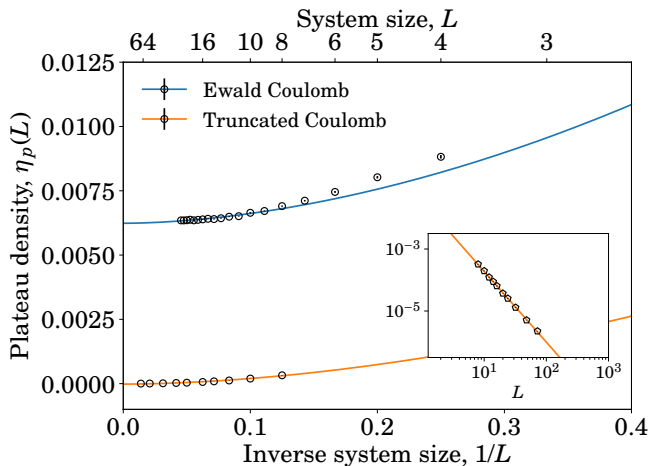


FIG. 11. Finite size scaling of the noncontractible plateau density $\eta_p(L)$ for the case of charges hopping on the diamond lattice subject to long-range Coulomb and truncated interactions. The data are averaged over at least 4096 histories. The lines are fits to the scaling ansatz $\eta_p(L) - \eta_p(\infty) \sim L^{-\nu}$, while the symbols represent the Monte Carlo data. The corresponding error bars are smaller than the width of the fit lines. As for CSI, the case of truncated interactions ($L = 6-72$ inclusive) is consistent with a vanishing plateau density in the thermodynamic limit, verified by the log-log plot of plateau density against linear system size L in the inset. Conversely, the long-range Coulomb case ($L = 4-22$ inclusive) exhibits a nonvanishing plateau density in the thermodynamic limit: $\eta_p(\infty) = 6.24(2) \times 10^{-3}$.

V. SUMMARY AND MEAN FIELD MODELLING

From our simulations we see that the behaviour of the four models in question is visibly similar. The key differences are: (i) the finite size scaling of the plateau is consistent with a finite versus a vanishing value in the thermodynamic limit in the case of long-range versus truncated interactions, respectively; moreover, in the case of long-range interactions, (ii) the decay of $\rho_f(t)$ is notably faster, and the variation with system size L is stronger (i.e., ν is significantly larger), in the charge simulations than in the spin ice simulations.

The scaling fits to the Monte Carlo data $\eta_p(L) - \eta_p(\infty) \sim L^{-\nu}$ give the values summarised in Tab. I. In the following, we show how one can understand this behaviour qualitatively and sometimes even quantitatively using mean field population dynamics to model the time evolution of the monopole/charge densities.

Regarding the discrepancy in the decay of the free monopole density, highlighted in point (ii) above, the most significant difference between the dynamics of the two models in the regime where monopoles are sparse is the existence of blocked directions in classical spin ice [20]. That is, for a given (isolated) free monopole, there always exists one of four directions (corresponding to the minority spin) along which the monopole cannot hop, as shown schematically in Fig. 12. Assuming that the direction of the local Coulomb field is distributed randomly over the unit sphere, the fraction of charges which are unable to lower their energy due to blocking is $\Omega_b/4\pi$, where Ω_b is the

solid angle for which there is a positive projection onto exactly one of the local basis vectors $\{e_i\}$. This leads to a probability

$$p_b = \frac{\Omega_b}{4\pi} = \frac{3}{2\pi} \left[\frac{\pi}{3} - \arctan \sqrt{2} \right] \approx 4.4\%, \quad (8)$$

for a given free monopole to be pinned (at zero temperature) due to blocking, as shown in App. D. In addition, even when the monopole is not pinned, the available phase space for motion is reduced by blocking. Notice that (8) underestimates the effect of pinning, because at the lattice scale the direction of the Coulomb interaction is correlated with the bond directions, which violates the assumption of uniformity over the unit sphere. Hence, we conclude that a finite fraction of monopoles, lower-bounded by (8), are instantaneously pinned in the spinful description due to blocked directions. It is then reasonable to expect that the free monopole density decays more slowly in the presence of such pinned charges. While this is an interesting aspect of stochastic processes in spin ice that warrants further investigation (maybe by including some effective disorder in the relevant charge population dynamics equations), it is beyond the scope of the present paper. We shall nonetheless see below that this effect plays a key quantitative role in the difference between long-range CSI and CM results.

In order to gain insight on the origin of the different behaviours observed in the various models, and to obtain estimates of the finite size scaling exponents to compare with our numerical results, we turn to mean field population dynamics of reaction diffusion processes.

A. Short-time dynamics

If we want to describe the simulations in terms of reaction-diffusion processes between (effective) particles, we ought to consider in principle five different species: positive and negative single and double charges, and noncontractible pairs. The noncontractible pairs are immobile, pinned to the bond on which they form. Single charges are able to move freely throughout the lattice (neglecting the effects of spin blocking/pinning). The double charges can either decay spontaneously into two single charges of the same sign if adjacent to an empty site, or they can be hit by a single charge of the opposite sign, and decrease their charge by one, thus producing a single (mobile) charge. Finally, two adjacent double charges of opposite sign can decay to form

| Model | Interactions | Plateau value, $\eta_p(\infty)$ | Scaling exponent, ν |
|-------|--------------|---------------------------------|-------------------------|
| CSI | truncated | 0 | 2.46(1) |
| | long-range | $4.7(9) 10^{-3}$ | 0.9(3) |
| CM | truncated | 0 | 2.28(2) |
| | long-range | $6.24(2) 10^{-3}$ | 1.8(4) |

TABLE I. Summary of finite size scaling results for both systems and both types of interaction between the tetrahedral charges. The scaling ansatz $\eta_p(L) - \eta_p(\infty) \sim L^{-\nu}$ was used to obtain the values shown in the table.

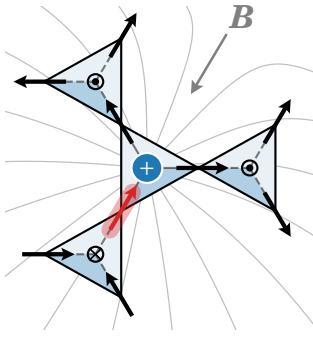


FIG. 12. Schematic depiction of a blocked direction for a free monopole. The isolated monopole is unable to move along the bond containing the minority spin (shown in red), since its reversal would lead to the creation of a double charge on the central tetrahedron. Blocked directions have a significant quantitative impact on the dynamics of monopoles subject to long-range interactions by instantaneously pinning some finite fraction of free monopoles. The local magnetic field \mathbf{B} determines which direction(s) lower the energy of the system; if this direction is unique and coincides with the blocked direction (as in the figure), then the monopole is pinned.

a noncontractible pair by flipping the intervening spin. All processes reduce the energy of the system, and thence are able to occur spontaneously even at zero temperature. The rate of decay of double monopoles does depend on the free monopole density, however it is easy to convince oneself that the ‘phase space’ for decay (either spontaneous or monopole-assisted) is always larger than that for processes which preserve the number of double charges, and it becomes progressively more so as free monopoles decay in time. Their evolution thus rapidly decouples from the other species and becomes exponentially fast in time: $\rho_d(t) \propto e^{-7t/2}$, as argued in App. C, which appears to fit well all simulations.

The single charges that are produced in the decay of double charges merely become a known time-dependent source term in the corresponding equation for the population dynamics of the single charges; as we see from the simulations, this contribution becomes irrelevantly small for $t \gtrsim 1$. When looking at the total or free monopole/charge densities, the double charges contribute towards the ‘hump’ observed at short times, before the onset of the asymptotic power-law behaviour. In App. C we discuss this in greater detail, and we show explicitly that the double charge contribution indeed does not affect the asymptotic scaling behaviour we are interested in understanding, only affecting the (non-universal) value of the noncontractible plateau.

Hence, in the following, we shall ignore the double charges altogether and focus on the three remaining species of particles: positively and negatively charged free monopoles living on the sites of a diamond lattice, with densities $\rho_q(t)$ (charge $q = \pm$); and immobile noncontractible pairs living on the bonds, with density $\eta(t)$. The equations governing their dynamics are presented and analysed in the following sections.

B. Truncated interactions

The mean field equations (i.e., neglecting spatial fluctuations) describing the time evolution of the monopole densities in the case of truncated interactions between monopoles are

$$\frac{d\rho_q}{dt} = -\mathcal{K}\rho_+\rho_-, \quad (9)$$

$$\frac{d\eta}{dt} = -\frac{\mathcal{R}}{2}(\rho_+ + \rho_-)\eta + \mathcal{K}'\rho_+\rho_-. \quad (10)$$

The first equation describes the annihilation of oppositely charged free monopoles, which occurs with rate \mathcal{K} . The first term in the second equation, with rate \mathcal{R} , describes the radioactive decay of noncontractible pairs—a free monopole annihilates the member of a noncontractible pair with the opposite sign. Such a process removes two monopoles previously forming a noncontractible pair, but preserves the number of free monopoles in the system, and therefore does not appear in (9). Finally, the second term in (10) describes the probabilistic formation of noncontractible pairs when two oppositely charged monopoles come into nearest-neighbour contact. As we want to understand the origin and scaling behaviour of the noncontractible pair plateau, we are not interested in the very long-time behaviour of the system. We have therefore disregarded the terms corresponding to the activated decay of the noncontractible pairs. Equivalently, (9) and (10) describe the zero-temperature dynamics of the system.

Charge neutrality ensures that $\rho_+(t) = \rho_-(t)$ for all times, allowing us to solve (9) for the time evolution of the free monopole densities $\rho_q(t)$:

$$\rho_q(t) = \frac{\rho_q^0}{1 + \mathcal{K}\rho_q^0 t}, \quad (11)$$

where $\rho_q^0 \equiv \rho_q(0)$. This solution may then be substituted into (10) describing the noncontractible monopole density $\eta(t)$

$$\frac{d\eta}{dt} + \mathcal{R}\rho_q(t)\eta = \mathcal{K}'\rho_q^2(t), \quad (12)$$

which can also be solved exactly to give

$$\eta(t) = \frac{(\mathcal{K}'/\mathcal{K})\rho_q^0}{(\mathcal{R}/\mathcal{K} - 1)(1 + \mathcal{K}\rho_q^0 t)} + \left[\eta_0 - \frac{(\mathcal{K}'/\mathcal{K})\rho_q^0}{\mathcal{R}/\mathcal{K} - 1} \right] \frac{1}{(1 + \mathcal{K}\rho_q^0 t)^{\mathcal{R}/\mathcal{K}}}. \quad (13)$$

Evidently, the long-time behaviour of the noncontractible monopole density $\eta(t)$ depends crucially on the ratio of rate constants \mathcal{R}/\mathcal{K} . If $\mathcal{R}/\mathcal{K} < 1$, then the second term in (13) dominates at long times and the noncontractible pairs decay more slowly than the free monopoles, as is observed in the numerics, illustrated in particular in Figs. 5 and 10 (this is also consistent with the analytic estimates of \mathcal{R}/\mathcal{K} that we present below).

In the thermodynamic limit, these equations do not predict a plateau in the noncontractible pair density since both $\rho_q(t)$

and $\eta(t)$ may become arbitrarily small. However, in a system of finite size containing $8L^3$ tetrahedra, the decay of $\rho_q(t)$ is cut off when the free monopole density reaches $O(1/L^3)$: $\rho_q(t_*) \sim L^{-3}$, i.e., at a time $t_* \sim L^3$ corresponding to the removal of *all* free monopoles in a finite system. If the noncontractible pair density decays more slowly, as is the case for $\mathcal{R}/\mathcal{K} < 1$, there is still a finite density of noncontractible pairs present in the system at t_* , and they can further decay only via thermal activation. The value of this density scales as $\eta(t_*) \sim t_*^{-\mathcal{R}/\mathcal{K}}$ for sufficiently large $t_* \gg (\mathcal{K}\rho_q^0)^{-1}$, allowing us to deduce the leading behaviour of the noncontractible plateau with system size:

$$\eta(t_*) \sim L^{-3\mathcal{R}/\mathcal{K}}, \quad (14)$$

and therefore extract the exponent $\nu = 3\mathcal{R}/\mathcal{K}$.

We can estimate the ratio \mathcal{R}/\mathcal{K} from the microscopic details of our system as the product of two contributions,

$$\frac{\mathcal{R}}{2\mathcal{K}} = \frac{N_{\mathcal{R}}}{N_{\mathcal{K}}} \cdot \frac{\tau_{\mathcal{K}}}{\tau_{\mathcal{R}}} \simeq \frac{3}{4} \cdot \frac{1}{2}. \quad (15)$$

The first factor in (15), $N_{\mathcal{R}}/N_{\mathcal{K}}$, comes from the fact that a free monopole has 4 adjacent free legs along which another free monopole may approach, while a noncontractible pair has only 3 (one of the four total legs being blocked by the other member of the pair) [21]. Therefore the factor 3/4 encapsulates the relative sizes of the basins of attraction in the two cases. The second factor $\tau_{\mathcal{K}}/\tau_{\mathcal{R}}$ derives from the ratio of timescales—in the case where two free monopoles are approaching one another, both are mobile, while in the case of a free monopole approaching a noncontractible pair, the noncontractible pair is pinned and only the free monopole is mobile. This leads to a factor of 2 difference in the (random walk) timescales for the two processes. The factor of 1/2 on the left hand side of (15) originates from the definition of \mathcal{R} in (10). We therefore estimate that $\mathcal{R}/\mathcal{K} \simeq 3/4$, and correspondingly the noncontractible plateau scales approximately as

$$\eta(t_*) = \eta_p(L) \sim L^{-9/4}, \quad (16)$$

in the case of truncated interactions between charges.

This estimate can be improved upon by examining larger clusters. Indeed, including next nearest neighbours in the cluster, the presence of blocked directions leads to a small correction to the finite size scaling exponent in the case of CSI, while it remains unchanged for the CM:

$$\nu_{\text{CSI}} = \frac{90}{37} \simeq 2.43, \quad \nu_{\text{CM}} = \frac{9}{4} = 2.25. \quad (17)$$

These exponents are consistent with the values $\nu = 2.46(1)$ and $\nu = 2.28(2)$ obtained in the spinful and Coulomb gas simulations, respectively. Note that the absolute values of \mathcal{R} and \mathcal{K} differ substantially between CSI and the CM due to the presence of blocked directions in the former, but their *ratio* remains essentially constant.

We are now able to understand why the spinful and charge descriptions exhibit quantitatively similar behaviour. In both cases, the charges exhibit diffusive motion (until they become

nearest neighbours, at which point they deterministically annihilate). The numerical results suggest that the annealed (random) blocked directions do not significantly affect the diffusive motion of the charges, and therefore do not alter the form of the decay of the free monopole density. This is because the motion of monopoles across the system (i.e., beyond nearest-neighbour separation) is not subject to any energetic bias controlling the direction of their motion. Hence, the insertion of blocked directions at random has little effect on the purely random motion of charges when averaged over histories—no monopoles are instantaneously pinned due to blocking. The free monopole density therefore decays as $1/t$ in both cases and we get a vanishing plateau in the thermodynamic limit. Further, the value of ν is set by the ratio of the rates of radioactive decay to free monopole decay, which is common to both descriptions, up to small corrections which result from the impact of blocked directions on the microscopic annihilation process.

C. Long-range coulomb interactions

In Sec. VB we were able to develop a rather complete understanding of the case of truncated interactions, which largely hinged on the $1/t$ scaling of the free monopole density. We would now like to study how the behaviour changes in the presence of long-range interactions. One could naively try to introduce them at the level of the reaction diffusion equations; however, this is known to recover the law of formal kinetics at long times, i.e., $1/t$ behaviour of $\rho_f(t)$, which leads to the same conclusion of a vanishing plateau value in the thermodynamic limit. This is however in contradiction with the observation that $\rho_f(t)$ decays faster than $1/t$ in our Monte Carlo simulations of long-range interacting systems.

As is often the case, the devil lies in the details. In order to observe a long-lived metastable plateau, we need to quench to very low temperatures, $T \ll J_{\text{eff}}$. In a discrete system with long-range interactions and finite lattice spacing, the hydrodynamic description of Refs. 8 and 22 does not always apply to the Monte Carlo time evolution of our simulations. Take the limiting case of a quench to zero temperature. The quasiparticles move only downwards or across in energy, $\delta E \leq 0$, and they move at ‘terminal velocity’ (i.e., one lattice spacing per unit time) irrespective of the strength of the force acting upon them. On the contrary, the hydrodynamic description applies when the Monte Carlo process is a (lightly) biased random walk, $|\delta E| \ll T$, and the equations of motion approximately take the familiar overdamped form where the velocity of the particles is proportional to the force acting on them. This is how our simulations violate the law of formal kinetics (at intermediate times) and achieve a decay of free monopole density which is faster than $1/t$ at the low temperatures studied in this manuscript.

Modelling the strictly-biased motion at terminal velocity is a tall order. However, at mean field level, one can put forward the following approximate argument: the free monopole density decays with a time constant given by the time taken to travel at terminal velocity to the next free monopole, some characteristic distance $\rho^{-1/d}$ away, namely $\tau_{\text{tv}} \sim \rho^{-1/d}$, where d is the

dimensionality of the system. Then we have

$$\frac{d\rho}{dt} \propto -\frac{\rho}{\tau_{\text{IV}}} \quad \Rightarrow \quad \rho(t) \sim 1/t^d. \quad (18)$$

This behaviour is in very good agreement with the $\rho_f(t)$ decay observed in the CM with long-range interactions if one neglects the formation of noncontractible pairs. We shall delay the discussion of the CSI case to later in this section.

In the absence of long-range interactions, there are no forces beyond a fixed finite separation between monopoles and they perform an unbiased random walk, even at zero temperature. It then takes a characteristic time, ρ^{-1} , corresponding to the time taken for a monopole to explore its characteristic volume in three dimensions to come in contact and annihilate with another. In this case, τ_{IV} should be replaced by $\tau_{\text{rw}} \sim \rho^{-1}$ and one recovers the $1/t$ scaling obtained more rigorously in Sec. VB.

In order to express all these considerations more formally, and to take into account explicitly the noncontractible pair density $\eta(t)$ which has been ignored thus far, it is convenient to introduce the following phenomenological reaction diffusion equations

$$\frac{d\rho_q}{dt} = -\mathcal{K}[\rho_+(t)\rho_-(t)]^{(1+\beta)/2}, \quad (19)$$

$$\frac{d\eta}{dt} = -\frac{\mathcal{R}}{2}(\rho_+ + \rho_-)\eta - \frac{\mathcal{K}'}{\mathcal{K}} \frac{d\rho_q}{dt}, \quad (20)$$

with the parameter $\beta \leq 1$ (with $\beta = 1$ corresponding to the truncated case, and $\beta = 1/3$ corresponding to the terminal velocity argument given above, neglecting the effect of nonzero η).

Using charge neutrality $\rho_+(t) = \rho_-(t)$, the first of these equations gives rise to a free monopole density

$$\rho_q(t) = \frac{\rho_q^0}{(1 + \beta\mathcal{K}_0\rho_q^0 t)^{\beta-1}}, \quad (21)$$

where we have defined for convenience $\mathcal{K}_0 \equiv \mathcal{K}(\rho_q^0)^{\beta-1}$ (and similarly for \mathcal{K}'_0). The parameter β sets the asymptotic rate of decay of the free monopole density in the system: $\rho_q(t) \sim t^{-\beta-1}$. This decay is faster than the truncated case ($1/t$) when $\beta < 1$. Defining

$$\Theta(t) = \int_0^t dt' \rho_q(t') \quad (22)$$

$$= \frac{1}{1-\beta} \frac{1}{\mathcal{K}_0} \left[1 - (1 + \beta\mathcal{K}_0\rho_q^0 t)^{-(\beta-1)/\beta} \right], \quad (23)$$

the solution for the noncontractible monopole density may be written as

$$\eta(t) = e^{-\mathcal{R}\Theta(t)} \left[\eta_0 + \int_0^t dt' e^{\mathcal{R}\Theta(t')} \mathcal{K}'[\rho_+(t')\rho_-(t')]^{(1+\beta)/2} \right]. \quad (24)$$

It is possible to obtain an analytic expression for $\eta(t)$ by expressing the integral in (24) in terms of the incomplete Gamma function, which is presented in Appendix B. Since,

for $\beta < 1$, $\Theta(t)$ tends towards a constant at large times, the solution for $\eta(t)$ exhibits a plateau at finite density, $\eta(t) \rightarrow \eta_\infty$, as $t \rightarrow \infty$. The density at which this plateau occurs is

$$\eta_\infty = e^{-\alpha\mathcal{R}/\mathcal{K}_0} \left\{ \eta_0 + \rho_q^0 \frac{\alpha\mathcal{K}'}{\mathcal{K}} e^{\alpha\mathcal{R}/\mathcal{K}_0} \left[\frac{\alpha\mathcal{R}}{\mathcal{K}_0} \right]^{-\alpha} \gamma \left(\alpha, \frac{\alpha\mathcal{R}}{\mathcal{K}_0} \right) \right\}, \quad (25)$$

where $\alpha \equiv 1/(1-\beta)$, and $\gamma(s, x)$ is the lower incomplete gamma function. Hence, the value of the plateau is exponentially sensitive to the ratio of rate constants $\mathcal{R}/\mathcal{K}_0$.

At sufficiently large times,

$$\eta(t) \simeq \eta_\infty \left[1 + \frac{\alpha\mathcal{R}}{\mathcal{K}_0} (\beta\mathcal{K}_0\rho_q^0 t)^{(\beta-1)/\beta} \right]. \quad (26)$$

The finite size scaling of the noncontractible plateau then follows from the fact that the free monopole decay is cut off at a time t_* , defined by $\rho_q(t_*) \sim L^{-3}$. As before, t_* equals the time at which free monopoles are completely removed from a system of finite size. This gives $t_* \sim L^{3\beta}$ and correspondingly the finite size scaling of the plateau satisfies

$$\eta(t_*) - \eta_\infty \sim t_*^{-(1-\beta)/\beta} \sim L^{-3(1-\beta)}. \quad (27)$$

The scaling exponent of the plateau, ν , can therefore be directly related to the exponent β which quantifies the asymptotic rate of decay of the free monopole density, i.e.,

$$\nu = 3(1 - \beta). \quad (28)$$

This relationship is consistent with the discrepancy between the finite size scaling exponents in the CSI and CM cases: the rapid decay of the free monopole density permitted by the lack of blocked directions in the CM case implies a larger β^{-1} and, hence, a larger ν . Indeed, evaluating the exponent of the asymptotic free monopole decay, we obtain $\beta^{-1} \simeq 1.4$ and $\beta^{-1} \simeq 2.3$ corresponding, through (28), to scaling exponents $\nu \simeq 0.86$ and $\nu \simeq 1.7$ for the cases of CSI and the CM, respectively. These values are in reasonable agreement with those obtained from the numerical finite size scaling analysis: $\nu = 0.9(3)$ and $\nu = 1.8(4)$.

Notice that the mean field equations (19) and (20) can only be expected to hold at asymptotically long times for zero-temperature quenches. For any finite T , as the monopoles become sparser, the forces between them become weaker and eventually one reaches the hydrodynamic regime, $|\delta E| \ll T$, discussed earlier, and a $1/t$ decay of $\rho_f(t)$ ensues. The typical (unsigned) Coulomb interaction felt by a given monopole through the separation $\rho(t)^{-1/d}$ is (in $d = 3$ for concreteness)

$$\langle E_c(t) \rangle \sim E_{\text{nn}} \rho(t)^{1/3}. \quad (29)$$

The corresponding *change* in Coulomb energy when moving a free monopole to an adjacent site then scales as

$$\langle \delta E_c(t) \rangle \sim E_{\text{nn}} \rho(t)^{2/3}. \quad (30)$$

Assuming $\rho(t) \sim 1/t^{\beta-1}$, the time threshold $\langle \delta E_c(t) \rangle \sim T$ corresponding to the crossover to $1/t$ decay of ρ_f can then be estimated to scale with temperature as $t_T \sim (E_{\text{nn}}/T)^{3\beta/2}$.

This crossover is observed in our Monte Carlo simulations at sufficiently high temperatures (not shown). From (20), we deduce that the noncontractible plateau therefore begins to decay at times $t \gtrsim t_T$. The rate of decay however vanishes with vanishing temperature, i.e., $\ln \eta \sim -T^{\nu/2} \ln t$. The zero temperature limit therefore does not commute with the infinite time limit. If the latter is taken first, the plateau decays to a vanishing thermodynamic value at large times. If the former is taken first, then a finite plateau survives. Since the timescale for activated decay of the plateau scales exponentially with temperature, while t_T scales algebraically [at least for a power law decay of $\rho_f(t)$], it will be the case that $t_T < \exp(\Delta/T)$ at the low but finite quench temperatures that we considered in this manuscript. For systems of finite size, the relevant question then becomes whether t_T is larger or smaller than the time t_* that it takes for the free monopole density to become less than $O(1/L^3)$.

We finally note that even at zero temperature the mean field equations will eventually break down at a time corresponding to single charge densities ρ_q at which free charges become so dilute that the bias for free charge–charge annihilation over radioactive decay is removed. We term such a time t_d , which may be obtained by comparing $\langle \delta E_c(t) \rangle$ with the typical energy due to charge–dipole interactions with the noncontractible pairs present in the noncontractible plateau. Once this bias is removed, radioactive decay may once again become favourable and the plateau is able to gradually decay.

The phenomenological model that we have presented illustrates in a simple manner the mechanisms at play, but we note that the precise functional form or even the asymptotic power law decay of the free monopole density implied by the model are not a requirement in order to observe a noncontractible plateau in the thermodynamic limit. Indeed, at the mean field level, *any* decay of $\rho_f(t)$ faster than $1/t$ will give rise to a plateau in the density of monopoles forming noncontractible pairs. Even if $\rho_f(t)$ does exhibit a crossover to $1/t$ behaviour at long times, the plateau will still be present in the thermodynamic limit, but will only exist for a finite period of time before it starts to decay.

VI. CONCLUSIONS

We have shown using a combination of Monte Carlo simulations and detailed mean field modelling that the metastable plateau which results from thermal quenches to low temperatures in classical spin ice is a consequence of the long-range Coulomb nature of the interactions between monopoles combined with the system entering a non-hydrodynamic regime which is controlled by nonuniversal lattice physics. The claim that such a plateau may have been observed in recent experiments [5] provides further compelling evidence for the long-range nature of the interactions between the emergent monopoles in classical spin ice.

In particular, we have shown that when the interactions between the monopoles are truncated to finite range, the plateau reduces to a finite size effect. This is because the free monopoles in the system perform independent random walks (when their

density is sufficiently low) leading to a slow $1/t$ decay of their density with time t . This is insufficient to create the “population inversion” required for the metastable plateau in the thermodynamic limit, since monopole-assisted (radioactive) decay remains effective and continues to remove noncontractible pairs from the plateau indefinitely.

When the full Coulomb interaction between monopoles is reinstated, there exists an energetic bias in the motion of monopoles across the system. At sufficiently low temperatures, which are relevant for the formation of a thermodynamic noncontractible plateau, the system enters a non-hydrodynamic regime where the monopoles move at terminal velocity in the direction of the local force acting on them. This combination of long-range interactions and non-hydrodynamic behaviour leads to a rapid decay of the free monopole density, faster than $1/t$ and violating the law of formal kinetics. The decay of free monopoles is then sufficiently rapid to stop the radioactive decay of noncontractible pairs at long times, and therefore one observes a plateau of finite density in the thermodynamic limit.

The potential departure of long-range interacting lattice systems from a hydrodynamic description, and thence from the law of formal kinetics, is somewhat expected: at sufficiently low temperatures, the change in energy incurred by a microscopic discrete update in the system becomes larger than the thermal energy. However, one generally expects this phenomenon to affect only the short-time transient dynamics, and at long times the universal hydrodynamic behaviour is recovered. Thermal quenches in spin ice demonstrate that, while this expectation must ultimately be satisfied, the altered nonuniversal, transient dynamics can induce very long-lived metastable states that change the behaviour of the system over a large range of ‘intermediate’ times spanning many orders of magnitude.

This phenomenon may play a role in other aspects of the behaviour of spin ice models and materials at low temperature (for example, a departure from hydrodynamic behaviour could be a contributing factor to the deviation from the so-called ‘quasiparticle kinetics’ in Ref. 5). It may also be relevant to other long-range interacting natural and artificial lattice systems of interest.

ACKNOWLEDGMENTS

CC is particularly grateful to R. Moessner, with whom the seed ideas behind this project were formulated. The authors would also like to thank P. Krapivsky, C. Laumann and G. Goldstein for insightful discussions. This work was supported in part by the Engineering and Physical Sciences Research Council (EPSRC) Grants No. EP/K028960/1, EP/M007065/1, and EP/P034616/1. This project was carried out using resources provided by the Cambridge Service for Data Driven Discovery (CSD3) operated by the University of Cambridge Research Computing Service (<http://www.csd3.cam.ac.uk/>), provided by Dell EMC and Intel using Tier-2 funding from the Engineering and Physical Sciences Research Council (capital grant EP/P020259/1), and DiRAC funding from the Science and Technology Facilities Council (www.dirac.ac.uk).

Appendix A: Simulation Details

Ewald summation leads to the following expression for the Coulomb energy of a set of interacting charges $\{q_a\}$ and their periodic images

$$E_c(\{q_a\}) = \sum_{a>b} q_a K_{ab} q_b + \mu \sum_a q_a^2, \quad (\text{A1})$$

where we have defined $K_{aa} \equiv 0, \forall a$, having separated out the diagonal terms, which may be absorbed into the effective chemical potential for charges. Supposing that we flip a spin S_i , the charges on the two adjacent tetrahedra, labelled by a, b , are modified: $q_a \rightarrow Q_a$, and $q_b \rightarrow Q_b$. The change in Coulomb energy when flipping this spin is therefore

$$\begin{aligned} \delta E_c(Q_a, Q_b) = & \sum_{c:q_c \neq 0} [\delta q_a K_{ac} + \delta q_b K_{bc}] q_c \\ & + \delta q_a K_{ab} \delta q_b + \mu [\delta(q_a^2) + \delta(q_b^2)], \quad (\text{A2}) \end{aligned}$$

where $\delta q_a = Q_a - q_a$, and $\delta(q_a^2) = Q_a^2 - q_a^2$. Such an expression already represents an improvement over the conventional dipolar Monte-Carlo code—one needs only to sum over the nonzero charges, which are dilute in the metastable plateau.

However, one can further speed up the computation of the Coulomb energy by considering the *change* in the Coulomb spin flip energies when going from time step $t \rightarrow t+1$. Suppose that in the WTMC update at time t , spin S_j , adjacent to tetrahedra c, d , was flipped. We then propose flipping S_i , adjacent to tetrahedra a, b . If there is no overlap between a, b and c, d , the change in spin flip energy between time steps t and $t+1$ is simply

$$\delta E_c(t+1) - \delta E_c(t) = (\delta q_a \ \delta q_b) \begin{pmatrix} K_{ac} & K_{ad} \\ K_{bc} & K_{bd} \end{pmatrix} \begin{pmatrix} \delta q_c \\ \delta q_d \end{pmatrix}. \quad (\text{A3})$$

Computing the Coulomb energy using the above expression (A3) is substantially faster than (A2) since it involves an $O(1)$ number of terms as opposed to $O(L^3)$. If one or both of the tetrahedra a, b and c, d do overlap, then the expression (A3) must be modified, but it remains $O(1)$ in complexity per spin. Hence, the overall complexity scales as $O(L^3)$ per WTMC step.

The dipolar interaction between spins, $E_d = \sum_{i<j} S_i K_{ij} S_j$, can also be implemented in a similar way with $O(1)$ complexity per spin. Suppose that at time t the spin S_r was flipped, and we would like to then propose flipping S_k both before and after flipping spin S_r . We find that in the case $k \neq r$

$$\delta E_d^{(k)}(t+1) - \delta E_d^{(k)}(t) = -4S_k(t)K_{kr}S_r(t). \quad (\text{A4})$$

In the special case $k = r$, we are proposing to reverse the previous spin flip and therefore $\delta E_d^{(k)}(t+1) - \delta E_d^{(k)}(t) = -2\delta E_d^{(k)}(t)$.

The absolute values of the spin flip energies must be recomputed periodically using (A2), or the equivalent expression in the case of dipolar interactions between spins, in order to prevent the accumulation of numerical error.

For truncated interactions, we need not generate fresh waiting times for all the spins at each step—only those affected by the previous update [16]. Hence, the complexity in this case scales as $O(\ln L)$ per WTMC step, allowing much larger systems to be accessed.

Appendix B: Solution to the mean field equations

Making use of the integral

$$\int dx \frac{e^{-r/(1+x)^s}}{(1+x)^t} = \frac{r^{-(t-1)/s}}{s} \Gamma\left(\frac{t-1}{s}, \frac{r}{(1+x)^s}\right), \quad (\text{B1})$$

for $t > 1$, we find that the full time-dependence of the noncontractible pair density may be expressed in terms of the upper incomplete gamma function $\Gamma(s, x)$ as

$$\begin{aligned} \eta(t) = e^{-\mathcal{R}\Theta(t)} & \left\{ \eta_0 + \rho_q^0 \frac{\alpha \mathcal{K}'}{\mathcal{K}} \left(\frac{\alpha \mathcal{R}}{\mathcal{K}_0}\right)^{-\alpha} e^{\alpha \mathcal{R}/\mathcal{K}_0} \right. \\ & \left. \times \left[\Gamma\left(\alpha, \frac{\alpha \mathcal{R}}{\mathcal{K}_0} \left(1 + \beta \mathcal{K}_0 \rho_q^0 t\right)^{(\beta-1)/\beta}\right) - \Gamma\left(\alpha, \frac{\alpha \mathcal{R}}{\mathcal{K}_0}\right) \right] \right\}. \quad (\text{B2}) \end{aligned}$$

Note that the behaviour of $\Theta(t)$ determines whether or not a metastable plateau appears; if $\Theta(t)$ tends to a constant for large times then the system will necessarily exhibit a plateau in the noncontractible pair density $\eta(t)$. This function is plotted in the inset of Fig. 9 for comparison with the charge model with long-range interactions.

Appendix C: Double charges

In this Appendix we show that the presence of double monopoles does not significantly alter the conclusions of our mean field modelling in Sec. V of the main text. In particular, we show by explicitly solving the mean field equations governing the population dynamics of monopoles subject to truncated interactions in CSI in the presence of double charges that, although the value of the plateau (in a finite system) is altered, the finite size scaling exponent ν remains unchanged. We argue that this feature is true more generally—further modifications of the mean field equations may change the short-time dynamics of the free monopole density, but leave its asymptotic decay ($\propto 1/t$) unchanged. This implies that the exponents derived in Sec. V are in some sense universal, while the precise value of the plateau is not.

In addition to the species considered in Sec. V, we introduce two new densities, $d_q(t)$ (where $q = \pm$), which equal the fraction of sites that host a charge $Q = \pm 2$, respectively. Notice that a double charge can always decay by reacting with any of its neighbouring tetrahedra (be them empty, occupied by a single or by a double charge), with the only exception being when it neighbours a single charge of the same sign, in which case flipping the intervening spin merely swaps the single and double charge without annihilating either of them. In principle the time evolution of the double charges depends therefore on the evolution of the single monopole density. Indeed, the average number of bonds surrounding an isolated double charge $2q$ along which it is able to decay is $4(1 - \rho_q)$ at the mean field level, i.e., assuming that each site is independent. The *asymptotic* decay of the double monopole density is however determined by neighbouring double charges of opposite sign since the number of bonds along which the pair may decay is $7/2 - 3(\rho_q + \rho_{\bar{q}})/2$ per site. Therefore, for all but the shortest

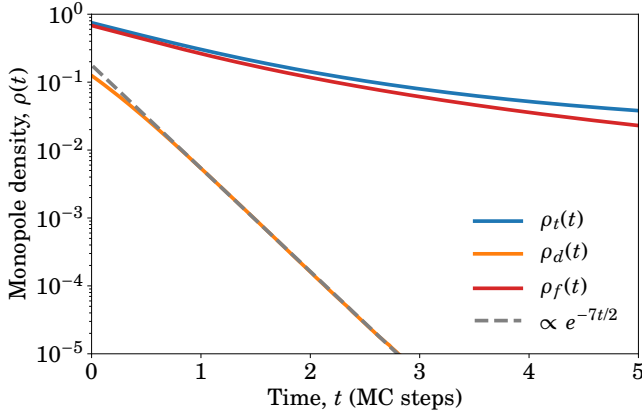


FIG. 13. Decay of the various monopole densities for a thermal quench from infinite temperature down to $T = 0.06$ K in spin ice (system size $L = 20$, i.e., 128 000 spins). The double charge density $\rho_d(t)$ decays exponentially with time with rate constant $\mathcal{K}_d = 7/2$. At very short times, $t \lesssim 1$, the effect of a nonzero free monopole density cannot be neglected, and the rate of double charge decay is reduced due to obstructed decay channels.

times where the effect of nonzero ρ_q cannot be neglected, we expect the double charge density to decouple from the other monopole densities and to decay exponentially with time constant $\mathcal{K}_d \approx 7/2$, i.e.,

$$\frac{d\rho_d}{dt} = -\mathcal{K}_d \rho_d. \quad (\text{C1})$$

Adding the two equations for $q = \pm$, we obtain $\rho_d(t) = \rho_d^0 e^{-\mathcal{K}_d t}$. This expectation is indeed confirmed by our Monte Carlo simulations of CSI, where we observe asymptotic exponential decay of the total double charge density $\rho_d(t) = d_+(t) + d_-(t)$ with time (see Fig. 13), consistent with the rate $\mathcal{K}_d = 7/2$.

The equation governing the free charge density ρ_q must also be modified to include the effect of double monopole decay:

$$\frac{d\rho_q}{dt} = -\mathcal{K}\rho_+\rho_- + 2\mathcal{K}'_d \rho_q(t). \quad (\text{C2})$$

The rate constant \mathcal{K}'_d corresponds to the spontaneous decay channel into adjacent empty sites only, implying that $\mathcal{K}'_d < \mathcal{K}_d$. Hence, the effect of including a nonzero density of double charges on the free monopole density is to add an exponentially decaying source term that corresponds to the production of free monopoles when double charges decay spontaneously. If we took into account spatial fluctuations, then we would also need to include a term $\propto (d_q \rho_{\bar{q}} - d_{\bar{q}} \rho_q)$ in this equation, but at the mean field level, charge neutrality of the single and double charges *separately* implies perfect cancellation of such a term. That is, when a single free charge q meets a double charge $2\bar{q}$, a free charge q is removed and a free charge \bar{q} is created. However, the rate at which this process occurs is identical for $q = \pm$. Substituting the exponential decay of $\rho_d(t)$ into this equation, we must solve the nonlinear equation

$$\frac{d\rho_q}{dt} + \mathcal{K}\rho_q^2 = \mathcal{K}'_d \rho_d^0 e^{-\mathcal{K}_d t}, \quad (\text{C3})$$

for $\rho_q(t)$, in which we have made use of charge neutrality, $\rho_+(t) = \rho_-(t)$. This equation has the exact solution

$$\rho_q(t) = y \frac{\mathcal{K}_d K_1(y) - c I_1(y)}{2\mathcal{K} K_0(y) + c I_0(y)}, \quad (\text{C4})$$

where we have written, for convenience of notation, $y(t) \equiv 2\sqrt{\mathcal{K}\mathcal{K}'_d \rho_d^0 / \mathcal{K}_d^2} e^{-\mathcal{K}_d t/2}$. The constant c is determined by the initial conditions $\rho_q(0) = \rho_q^0$, and $I_n(x)$ and $K_n(x)$ are modified Bessel functions of the first and second kind, respectively.

Finally, the expression for $\eta(t)$ must also be modified for direct comparison with our numerical results. When two double charges (of opposite sign) are adjacent to one another, the bond necessarily hosts one contractible pair and one noncontractible pair. The number of adjacent doubly occupied sites is simply proportional to $\rho_d(t)$, and the corresponding contribution to $\eta(t)$ contributes towards the kink in the noncontractible pair density observed in our numerical simulations at the characteristic decay time $t \sim \mathcal{K}'_d^{-1}$ of the double charges. At later times, the equation for $\eta(t)$ remains unchanged [23]

$$\frac{d\eta_1}{dt} = -\frac{1}{2}\mathcal{R}(\rho_+ + \rho_-)\eta_1 + \mathcal{K}'\rho_+\rho_-. \quad (\text{C5})$$

The form of the solution is

$$\eta(t) = e^{-\mathcal{R}\Theta(t)} \left[\eta(0) - \frac{\mathcal{K}'}{\mathcal{K}} \int_0^t dt' e^{\mathcal{R}\Theta(t')} \dot{\rho}_q(t') \right], \quad (\text{C6})$$

where we recall that $\Theta(t) \equiv \int_0^t dt' \rho_q(t')$. Hence, the asymptotic behaviour of $\eta(t)$ is directly determined by the asymptotic behaviour of $\rho_q(t)$. In order to derive this behaviour, we require the expansions of $I_n(x)$ and $K_n(x)$ for small values of the argument x [24]:

$$I_0(x) = 1 + O(x^2), \quad (\text{C7})$$

$$I_1(x) = \frac{1}{2}x + O(x^3), \quad (\text{C8})$$

$$K_0(x) = -\ln \frac{e^\gamma}{2}x + O(x^2 \ln x), \quad (\text{C9})$$

$$K_1(x) = \frac{1}{x} + \frac{1}{2}x \ln x + O(x), \quad (\text{C10})$$

where $\gamma \approx 0.5772$ is the Euler–Mascheroni constant. These expansions allow us to deduce that

$$\rho_q(t) = \frac{\mathcal{K}_d}{2\mathcal{K}} y \frac{1/y + (y/2) \ln y + O(y)}{\ln 2 - \ln e^\gamma y + c + O(y^2 \ln y)} \quad (\text{C11})$$

$$= \frac{1}{\mathcal{K}t} + O(t^{-2}), \quad (\text{C12})$$

independent of the initial conditions and independent of the initial rapid decay of double monopoles. The subleading term $\propto 1/t^2$ depends on this short-time dynamics through $\log y_0$ and through c . Correspondingly, for sufficiently large times,

$$\eta(t) \propto \frac{1}{(\mathcal{K}\rho_q^0 t)^{\mathcal{R}/\mathcal{K}}}. \quad (\text{C13})$$

The constant of proportionality is slightly renormalised in the presence of double charges since the asymptotic expansion of

the second term in (C6) depends on $\int_0^\infty dt e^{\mathcal{R}\Theta} \dot{\rho}_q$, which in turn depends on the full time-dependence of $\rho_q(t)$, including its short-time dynamics. However, the *exponent* ν is insensitive to such details [being determined by the exponents of the leading terms in (C12) and (C13)], and the scaling arguments presented in the main text remain robust to the addition of doubly occupied sites. That is, the precise value of the plateau is sensitive to the addition of double monopoles into the model, but the finite size scaling exponent $\nu = 3\mathcal{R}/\mathcal{K}$ remains unchanged.

Similarly, when the charges are subject to mutual Coulombic interactions, if the leading term in the asymptotic expansion of $\rho_q(t)$ remains proportional to $t^{-\beta-1}$, then the leading, time-independent term in $\Theta(t) = \text{const.} + O(t^{-(1-\beta)/\beta})$ will be sensitive to the presence of double charges. Therefore, since this term contributes to the value of the plateau in the thermodynamic limit, η_∞ from (25) will be modified slightly in the presence of doubly occupied sites. However, the subleading contribution ($\sim t^{-(1-\beta)/\beta}$), which determines the finite-size scaling exponent ν , will again be robust to the addition of doubly occupied sites, and the relation $\nu = 3(1-\beta)$, which relates the asymptotic decay of ρ_q to the finite size scaling behaviour, also remains unchanged.

More generally, adding further terms to our mean field equations (which depend on higher powers of the various densities) will indeed modify the short-time dynamics of $\rho_q(t)$. The precise density at which the plateau occurs in a system of finite size in the case of truncated interactions, and the value of the plateau in the thermodynamic limit in the case of long-range interactions depend—through (C6)—on the *full* history of $\rho_q(t)$, and therefore will be modified. However, the *asymptotic* behaviour of $\rho_q(t)$, which directly determines the finite-size scaling exponent ν for both types of interaction, is insensitive to such details.

Appendix D: Blocked directions

To derive the probability that a given monopole is pinned, it is convenient to use the following convention for the normalised

basis vectors:

$$\mathbf{e}_0 = \mathbf{e}_z, \quad (\text{D1})$$

$$\mathbf{e}_1 = \frac{2\sqrt{2}}{3}\mathbf{e}_x - \frac{1}{3}\mathbf{e}_z, \quad (\text{D2})$$

$$\mathbf{e}_2 = -\frac{\sqrt{2}}{3}(\mathbf{e}_x + \sqrt{3}\mathbf{e}_y) - \frac{1}{3}\mathbf{e}_z, \quad (\text{D3})$$

$$\mathbf{e}_3 = -\frac{\sqrt{2}}{3}(\mathbf{e}_x - \sqrt{3}\mathbf{e}_y) - \frac{1}{3}\mathbf{e}_z. \quad (\text{D4})$$

Now, the probability that a given monopole is instantaneously pinned, p_b , is $\Omega_b/4\pi$, where Ω_b is the solid angle over which there exists a positive projection onto exactly one of \mathbf{e}_μ ($\mu = 0-3$). In this case, there exists only one direction which lowers the energy of the monopole, and so the monopole will be pinned if the minority spin coincides with this direction.

For convenience, let us consider the solid angle Ω_0 corresponding to a positive projection onto \mathbf{e}_0 , and a negative projection onto the remaining three basis vectors. By symmetry, $\Omega_b = \Omega_0$. We therefore require that the following conditions are simultaneously satisfied

$$\cos \theta > 0, \quad (\text{D5})$$

$$2\sqrt{2} \sin \theta \cos \phi - \cos \theta < 0, \quad (\text{D6})$$

$$\sqrt{2}(-\sin \theta \cos \phi - \sqrt{3} \sin \theta \sin \phi) - \cos \theta < 0, \quad (\text{D7})$$

$$\sqrt{2}(-\sin \theta \cos \phi + \sqrt{3} \sin \theta \sin \phi) - \cos \theta < 0, \quad (\text{D8})$$

where we have parameterised the unit sphere using polar and azimuthal angles θ and ϕ , respectively. The corresponding solid angle defined by this region is (taking advantage of the D_3 symmetry about the z -axis)

$$\Omega_0 = 6 \int_0^{\pi/3} d\phi \int_0^{f(\phi)} d\theta \sin \theta \quad (\text{D9})$$

$$= 6 \int_0^{\pi/3} d\phi [1 - \cos f(\phi)], \quad (\text{D10})$$

where $f(\phi)$ is defined implicitly by the condition $2\sqrt{2} \sin f(\phi) \cos \phi - \cos f(\phi) = 0$, i.e., the limiting case of condition (D6). The other conditions (D7) and (D8) are also automatically satisfied if (D6) is satisfied in the region $0 < \phi < \pi/3$. Hence,

$$\cos f(\phi) = \frac{2\sqrt{2} \cos \phi}{\sqrt{1 + (2\sqrt{2} \cos \phi)^2}}, \quad (\text{D11})$$

and the integral (D10) over the azimuthal angle ϕ may be evaluated exactly to give

$$\Omega_0 = 6 \left[\frac{\pi}{3} - \arctan \sqrt{2} \right], \quad (\text{D12})$$

and finally $p_b = \Omega_0/4\pi$, giving the result stated in the main text.

- [1] S. T. Bramwell and M. J. P. Gingras, *Science* **294**, 1495 (2001).
- [2] C. Castelnovo, R. Moessner, and S. Sondhi, *Annual Review of Condensed Matter Physics* **3**, 35 (2012).
- [3] C. Castelnovo, R. Moessner, and S. L. Sondhi, *Nature* **451**, 42 (2008).
- [4] C. Castelnovo, R. Moessner, and S. L. Sondhi, *Phys. Rev. Lett.* **104**, 107201 (2010).
- [5] C. Paulsen, S. Giblin, E. Lhotel, D. Prabhakaran, G. Balakrishnan, K. Matsuhira, and S. Bramwell, *Nature Physics* **12**, 661 (2016).
- [6] C. Paulsen, M. J. Jackson, E. Lhotel, B. Canals, D. Prabhakaran, K. Matsuhira, S. Giblin, and S. Bramwell, *Nature Physics* **10**, 135 (2014).
- [7] S. Mostame, C. Castelnovo, R. Moessner, and S. L. Sondhi, *Proceedings of the National Academy of Sciences* **111**, 640 (2014).
- [8] A. A. Ovchinnikov and V. V. Atrazhev, *Physica A: Statistical Mechanics and its Applications* **276**, 1 (2000).
- [9] L. D. Jaubert and P. C. Holdsworth, *Nature Physics* **5**, 258 (2009).
- [10] R. Siddharthan, B. S. Shastry, A. P. Ramirez, A. Hayashi, R. J. Cava, and S. Rosenkranz, *Phys. Rev. Lett.* **83**, 1854 (1999).
- [11] B. C. den Hertog and M. J. P. Gingras, *Phys. Rev. Lett.* **84**, 3430 (2000).
- [12] This value of the effective exchange coupling was obtained using the chemical potential $\mu = -8.92$ K in Ref. [25]. In particular, we use $\mu = -4J_{\text{eff}} - E_{\text{nn}}$ to define J_{eff} . The dynamics of the system is however not particularly sensitive to the precise value of J_{eff} , as long as the ground state remains unchanged.
- [13] S. V. Isakov, R. Moessner, and S. L. Sondhi, *Phys. Rev. Lett.* **95**, 217201 (2005).
- [14] C. L. Henley, *Annual Review of Condensed Matter Physics* **1**, 179 (2010).
- [15] We note that defective tetrahedra in spin ice are also subject to Coulomb interactions of entropic origin [14]. Whereas we are unable to alter the range of such interactions, we generally expect them to be negligible. This is indeed confirmed by the good agreement between the CSI and CM results for truncated interactions.
- [16] J. Dall and P. Sibani, *Computer Physics Communications* **141**, 260 (2001).
- [17] J. Dall and P. Sibani, *The European Physical Journal B-Condensed Matter and Complex Systems* **36**, 233 (2003).
- [18] Note that there are many possible definitions of the ‘free’ monopole density due to ambiguities that arise in defining pairs of monopoles in the monopole-dense (short-time) limit. However, all definitions agree once the typical separation of monopoles is greater than r_{nn} .
- [19] As long as the final quench temperature satisfies $T \lesssim E_{\text{nn}}/L^2$, the dominant effect of changing temperature is to modify the long-time activated decay of the plateau. We therefore focus on the limit of zero temperature for simplicity.
- [20] One may also wonder whether the differences in the short-time dynamics affect significantly the asymptotic decay of the free monopole density. This has been ruled out by changing between the dynamics generated by long-range CSI and the long-range CM at some later time, say $t = 10$ (data not shown).
- [21] We note that in the spinful description, the rate constant \mathcal{K} includes the formation of noncontractible pairs in addition to annihilation events, and so blocked directions do not alter this argument to leading order.
- [22] V. V. Ginzburg, L. Radzihovsky, and N. A. Clark, *Phys. Rev. E* **55**, 395 (1997).
- [23] Including terms that correspond to the decay of neighbouring double charges into free monopoles gives rise to an exponentially decaying contribution to $\eta(t)$.
- [24] M. Abramowitz and I. Stegun, *Handbook of Mathematical Functions: With Formulas, Graphs, and Mathematical Tables*, Applied mathematics series (Dover Publications, 1965).
- [25] L. D. C. Jaubert and P. C. W. Holdsworth, *Journal of Physics: Condensed Matter* **23**, 164222 (2011).